Revisiting the mean-field picture of dipolar effects in solution NMR

Y. Morris Chen, R. T. Branca, and W. S. Warren
Department of Chemistry, Duke Box 90346, Duke University, Durham, North Carolina 27708, USA and Center for Molecular and Biomolecular Imaging, Duke University, Durham, North Carolina 27708, USA

(Received 16 December 2011; accepted 9 May 2012; published online 31 May 2012)

For more than three decades, the classical or mean-field picture describing the distant dipolar field has been almost always simplified to an effective field proportional to the local longitudinal magnetization, differing only by a scale factor of 1.5 for homomolecular (identical resonance frequency) and heteromolecular interactions. We re-examine the underlying assumptions, and show both theoretically and experimentally that the mathematical framework needs to be modified for modern applications such as imaging. We demonstrate new pulse sequences which produce unexpected effects; for example, modulating an arbitrarily small fraction of the magnetization can substantially alter the frequency evolution. Thus, matched gradient pulse pairs (a seemingly innocuous module in thousands of existing pulse sequences) can alter the time evolution in highly unexpected ways, particularly with small flip angle pulses such as those used in hyperpolarized experiments. We also show that specific gradient pulse combinations can retain only dipolar interactions between unlike spins, and the dipolar field can generate a secular Hamiltonian proportional to I_x. © *2012 American Institute of Physics*. [http://dx.doi.org/10.1063/1.4721637]

I. INTRODUCTION

Since the very beginnings of NMR, it has been known that dipolar couplings dominate the solid state linewidth for spin-1/2 nuclei[1,2] but the effects are still not fully understood: the full free induction decay has never been calculated, and recent experiments show an anomalously long lived component.[3,4] Diffusion in liquids[5] or quantum mechanical exchange in solid ^{3}He dramatically sharpens resonance lines by effectively decoupling nearby spins, but dipolar couplings can still produce effects in such systems.[6] The simplest case (uniform magnetization) was studied long before quantum mechanics: it is the origin, for example, of the "dipolar demagnetizing field" or "distant dipolar field" (DDF) which prevented certain shapes for permanent magnets, until the advent of modern materials with higher coercive force and remanence than pure iron.

Effects from uniform large magnetization are observable in NMR (Ref. 7) but are usually complicated by other nonlinear interactions, such as radiation damping. In contrast, it is very easy to spatially modulate magnetization with radiofrequency pulses and field gradients, and this leads to surprising experimental observations, such as multiple echoes in both solid ^{3}He (Ref. 6) and water.[8] Beginning in the mid-nineties, two-dimensional experiments revealed that dipolar couplings between distant spins produce strong signals from intermolecular multiple quantum coherences,[9,10] with a wide range of applications such as anisotropy measurement,[11–13] inhomogeneity compensation,[14,15] and temperature imaging.[16] The mathematical framework which describes these effects can be phrased in terms of nonlinear Bloch equations (the "mean-field picture," derived essentially unchanged from Ref. 6) or a density matrix framework which explicitly retains the dipolar couplings (the "coupled-spin picture"),[17] with identical results.[17–19]

Here we discuss simple pulse sequences (Figure 1) which produce signals that conflict dramatically with the accepted predictions. For example, the first two sequences in Figure 1 use a matched gradient pulse pair (used in thousands of existing, much more complex sequences) but as we show later, experimentally the signal is not the same as that of a simple free induction decay or spin echo; in fact, the evolution frequency during the time between the pulses depends on the gradient direction. Figure 1(c) looks like a simple modification to the double-quantum CRAZED sequence, but when the two pairs of gradient pulses are arranged along x and z, respectively (what we will call the XZ MAXCRAZED sequence) the experimental effects of couplings between like spins are eliminated, while the couplings between different spins are retained. Figure 1(d) looks like a simple modification to a COSY sequence, but if the second pair of gradient pulses is along any direction other than the magic angle, phase cycling of the first pulse reveals double-quantum peaks.

We also show the origin of the problem: seemingly intuitive simplifications which are virtually always used in the mean-field framework (and were propagated into the coupled-spin framework) need to be revisited. Specifically, the conventional treatment implicitly assumes that all components of the magnetization are strongly modulated in the same direction. This condition is violated in many sequences; for example, the transverse magnetization is modulated by readout and phase encode gradients in imaging sequences, but the z magnetization is not affected. We then generalize the traditional treatment of dipolar field effects. Our primary focus in this paper is developing a formalism that gives an intuitive explanation of the strange results from these sequences. Where it is possible, we will produce analytic solutions; we will also discuss cases where the analytic solutions break down, but a first-order result has predictive power. Finally, we discuss

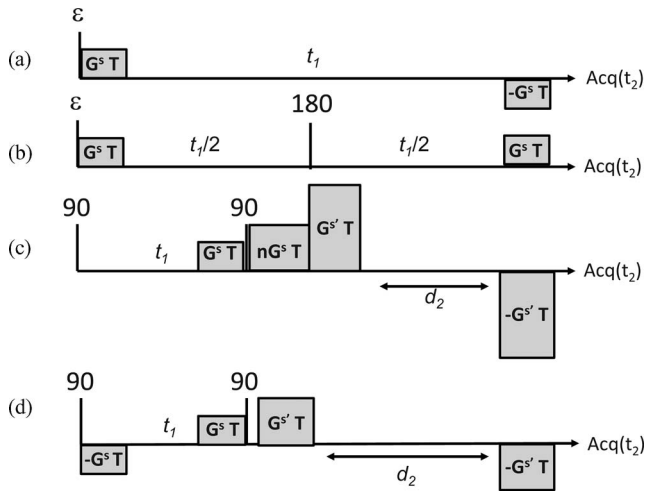

FIG. 1. Sequences which show limitations of the traditional mean-field picture of dipolar effects. In each case the vertical lines are rf pulses, and shaded boxes are gradient pulses along a specific direction s or s', with areas G^sT or $G^{s'}T$. (a) and (b): Here the first pulse flip angle ε is small, so almost all of the magnetization lies along the z axis. For a spherical sample, dipolar effects would then be expected to be unobservable. Instead, these sequences show a frequency shift determined by gradient direction, but independent of ε. Both experiments have identical dipolar effects; the second one suppresses inhomogeneous broadening and radiation damping. (c) MAXCRAZED sequence, which alters the CRAZED sequence by imposing strong gradients in a different direction during the interval d_2. Certain gradient pair directions dramatically alter the observed peaks. (d) GRACE sequence, which modifies a traditional COSY experiment by adding matched gradient pulse pairs in different directions in the two time intervals. Certain gradient pair directions produce double-quantum signals, as detected by phase cycling the first pulse.

the classes of experiments which are altered most by these corrections.

II. REVIEW OF CONVENTIONAL DIPOLAR FIELD TREATMENTS

We start by summarizing the conventional framework. The Hamiltonian reflecting the dipole-dipole interaction between nuclear spins i and j has the form

$$H_D = \frac{1}{2}\sum_{i,j}\frac{\hbar^2\gamma_i\gamma_j}{|\vec{r}_i-\vec{r}_j|^3}[\vec{I}_i\bullet\vec{I}_j-3(\vec{I}_i\bullet(\vec{r}_i-\vec{r}_j))\times(\vec{I}_j\bullet(\vec{r}_i-\vec{r}_j))/|\vec{r}_i-\vec{r}_j|^2]. \quad (1)$$

In a large external field $B_0\hat{z}$ this should be truncated (the "secular approximation") to retain only the components which commute with the Zeeman Hamiltonian.[1] The secular approximation to Eq. (1), in either the laboratory or rotating frame, is derived in standard textbooks:[2]

$$H_D = \frac{1}{4}\sum_{i,j}\frac{\hbar^2\gamma_i\gamma_j}{|\vec{r}_i-\vec{r}_j|^3}(1-3\cos^2\theta_{rr'})\times[3I_{zi}I_{zj}-\vec{I}_i\bullet\vec{I}_j] \quad (i,j \text{ homonuclear}) + \frac{1}{4}\sum_{i,j}\frac{\hbar^2\gamma_i\gamma_j}{|\vec{r}_i-\vec{r}_j|^3}(1-3\cos^2\theta_{rr'})\times[2I_{zi}I_{zj}] \quad (i,j \text{ heteronuclear}), \quad (2)$$

where $\theta_{rr'}$ is the angle between $\vec{r}-\vec{r}'$ and $\hat{z}$. The distinction between homonuclear and heteronuclear couplings arises because the resonance frequency difference between different nuclei is generally much larger than the dipolar couplings, and the component $I_{xi}I_{xj}+I_{yi}I_{yj}$ contained in the dot product only commutes with the Zeeman Hamiltonian if the resonance frequencies are equal.

In a groundbreaking paper, Ref. 6 extended this treatment to a system undergoing spin exchange (and the same approach was later extended to liquids[8]), where the couplings between nearby spins can be assumed to be averaged away by diffusion. The sum in Eq. (1) is replaced by an integral to account for distant spins, and the interaction can be reduced to what is today called the DDF at each position from all of the other spins,

$$\vec{B}_d(\vec{r}) = \frac{\mu_0}{4\pi}\int d^3r'\frac{1}{|\vec{r}-\vec{r}'|^3}[\vec{M}(\vec{r}')-3(\vec{M}(\vec{r}')\bullet(\vec{r}-\vec{r}'))\times(\vec{r}-\vec{r}')/|\vec{r}_i-\vec{r}_j|^2]. \quad (3)$$

Reference 6 then makes the same secular approximation as was done to get to Eq. (2), saving only terms in $\vec{B}_d(\vec{r})$ along the z axis or parallel to $\vec{M}(\vec{r}')$:

$$\vec{B}_d(\vec{r}) = \frac{\mu_0}{4\pi}\int d^3r'\frac{1-3\cos^2\theta_{rr'}}{2\,|\vec{r}-\vec{r}'|^3}[3M_z(\vec{r}')\hat{z}-\vec{M}(\vec{r}')], \quad (4)$$

where now the DDF affects the time evolution as an additional field source in the Bloch equations, $d\vec{M}/dt=\gamma(\vec{M}\times\vec{B})$ where $\vec{B}=B_0\hat{z}+\vec{B}_d(\vec{r})$.

There are a few analytical solutions for Eq. (4) (for example, the field from a spherical sample is zero inside the sphere, and equivalent to the field from a point dipole outside the sphere),[20] but in general the dipolar field predicted by the integral in Eq. (4) is nonlocal with components in all directions. Thus, for example, fluctuations in the magnetization density can create a dipolar field from even a spherical sample,[21,22] particularly with large magnetization, and such effects lead to highly nonreproducible signals in certain experiments. However, a very common special case is magnetization modulated in a single direction, for example, by gradient pulses. Fortunately, the dipolar field is simple and local[6] in reciprocal space after Fourier transformation of $\vec{B}_d$ and $\vec{M}(\vec{r})$:

$$\vec{B}_d(\vec{k}) = \mu_0[(3(\hat{k}\bullet\hat{z})^2-1)/2][M_z(\vec{k})\hat{z}-\vec{M}(\vec{k})/3]. \quad (5)$$

If the magnetization is completely modulated along a direction $\hat{s}$, the numerical factor in the first brackets of Eq. (5) is identical for all of the spatial frequency components, and then inverse Fourier transformation gives

$$\vec{B}_d(\vec{r}) = \mu_0\Delta(M_z(\vec{r})\hat{z}-\vec{M}(\vec{r})/3) = \mu_0\Delta(2M_z(\vec{r})\hat{z}-M_x(\vec{r})\hat{x}-M_y(\vec{r})\hat{y})/3, \quad (6)$$

where $\Delta=(3(\hat{s}\bullet\hat{z})-1)/2$.

Finally, since $d\vec{M}/dt=\gamma(\vec{M}\times\vec{B})$ the term proportional to $\vec{M}$ does not affect the evolution. Thus we can add a term proportional to $\vec{M}$, which if chosen correctly can produce a simpler "effective dipolar field" with the same evolution. Specifically, we can null out the modulated transverse

components, giving an effective dipolar field of the form

$$\vec{B}_{d,eff}(\vec{r}) = \mu_0 \Delta M_z(\vec{r})\hat{z} \quad \text{(homomolecular)}. \tag{7}$$

Equation (7) leads to a very simple picture: the effective dipolar field creates a frequency shift, proportional to the magnetization along the z axis. Here we have added the notation "homomolecular" to indicate the assumption that all of the spins have the same resonance frequency, including chemical shift. Because the retained solution dipolar couplings are small, even two different protons (e.g., water and acetone at normal magnetic field strengths) correspond to the "heteromolecular" case, but the generalization of Eqs. (4) and (7) is directly analogous to the homonuclear/heteronuclear distinction in solids,

$$\vec{B}_{d,eff}(\vec{r}) = \frac{\mu_0}{4\pi}\int d^3r' \frac{1-3\cos^2\theta_{rr'}}{2\,|\vec{r}-\vec{r}'|^3} \times [2M_z(\vec{r}')\hat{z}] \quad \text{(heteromolecular)}, \tag{8}$$

$$\vec{B}_{d,eff}(\vec{r}) = \frac{2\mu_0}{3}\Delta M_z(\vec{r})\hat{z} \quad \text{(heteromolecular)}. \tag{9}$$

This framework described above (and particularly the effective dipolar field picture in Eqs. (7) and (9)), has been used to describe a wide variety of experiments with dipolar fields, in part because it is often analytically solvable.[10,23] As a specific example, consider the n-quantum CRAZED sequence (Figure 2(a)). The superscript "s" designates the spatial direction of the gradient pulse (more precisely, the generated field when the gradient is on satisfies the relationship $\partial B_z/\partial s = G^s$ with the partial derivatives in all directions perpendicular to $\hat{s}$ vanishing). Relaxation, radiation damping and diffusion processes will be ignored, and for compactness we will assume that the gradient pulse durations are negligible, and treat the pulses as part of t_1 and t_2, respectively. Since there is no z-magnetization during the t_1 period and the first gradient, the effective dipolar demagnetizing field is zero during t_1. If both pulses have phase y, the magnetization after the second $\pi/2$ pulse is given by

$$\begin{aligned} M_z &= -M_0\cos[\omega\, t_1 + \gamma G^s T s]; \\ M^+ &= i\,M_0\sin[\omega\, t_1 + \gamma G^s T s], \end{aligned} \tag{10}$$

where ω is the resonance offset and $M^+ = M_x + iM_y$ is used instead of the individual components because it significantly simplifies the equations. During the second gradient and the t_2 period, the z-component of the magnetization stays constant in time and the x- and y-components evolve

$$\begin{aligned} M^+ &= e^{i\omega t_2}e^{in\gamma G^s T s}\exp\{i\gamma\mu_0 M_z \Delta t_2\} \\ &\quad \times i\,M_0\sin(\omega\, t_1 + \gamma G^s T s) \\ &= e^{i\omega t_2}e^{in\gamma G^s T s}\exp\{-i\gamma\mu_0 M_0 \Delta t_2\cos(\omega\, t_1 + \gamma G^s T s)\} \\ &\quad \times i\,M_0\sin(\omega\, t_1 + \gamma G^s T s). \end{aligned} \tag{11}$$

The term in curly brackets reflects evolution under the effective dipolar field. Using the Bessel function expansion $\exp(iz\cos\theta) = \sum_{m=-\infty}^{\infty} i^m J_m(z)e^{im\theta}$ gives

$$\begin{aligned} M^+ &= e^{i\omega t_2}e^{in\gamma G T z}\,i\,M_0\sin\left(\omega\, t_1 + \gamma G^s T s\right)\sum_{m=-\infty}^{\infty} i^m J_m\left(-t_2\Delta/\tau_d\right)e^{im\,\omega t_1 + im\gamma G^s T s} \\ &= e^{i\omega t_2}\frac{M_0}{2}\left(\begin{array}{l} \displaystyle\sum_{m=-\infty}^{\infty} i^m J_m\left(-t_2\Delta/\tau_d\right)\left[e^{i(m+1)\,\omega\, t_1 + i(n+m+1)\gamma G^s T s}\right] \\ \displaystyle -\sum_{m=-\infty}^{\infty} i^m J_m\left(-t_2\Delta/\tau_d\right)\left[e^{i(m-1)\,\omega\, t_1 + i(n+m-1)\gamma G^s T s}\right] \end{array}\right) \\ &= e^{i\omega t_2}\frac{M_0}{2}\left(\begin{array}{l} \displaystyle\sum_{m=-\infty}^{\infty} i^{m-1} J_{m-1}\left(-t_2\Delta/\tau_d\right)\left[e^{im\,\omega t_1 + i(n+m)\gamma G^s T s}\right] \\ \displaystyle -\sum_{m=-\infty}^{\infty} i^{m+1} J_{m+1}\left(-t_2\Delta/\tau_d\right)\left[e^{im\,\omega t_1 + i(n+m)\gamma G^s T s}\right] \end{array}\right) \\ &= e^{i\omega t_2}M_0\left(\sum_{m=-\infty}^{\infty} i^{m+1}\left(m\left(\tau_d/t_2\Delta\right)J_m\left(-t_2\Delta/\tau_d\right)\right)\left[e^{im\,\omega t_1 + i(n+m)\gamma G^s T s}\right]\right) \end{aligned} \tag{12}$$

Here we have introduced the demagnetizing time $\tau_d = (\gamma\mu_0 M_0)^{-1}$; for water at 7T (300 MHz) and 298K, $\tau_d = 130$ ms. Since the function $n\,J_n(x)/x \to 0$ as $x \to 0$ except for $n = \pm 1$, the transverse magnetization initially has only two Fourier components, modulated as $e^{i(n\pm1)\gamma G^s T s}$. Dipolar evolution creates signal, as the component with $n = -m$ is unmodulated,

$$\langle M^+(t_1,t_2)\rangle = i^{n-1}e^{i\omega t_2}e^{-in\omega t_1}M_0 n\left(\frac{\tau_d}{t_2\Delta}\right)J_n\left(\frac{t_2\Delta}{\tau_d}\right), \tag{13}$$

but it also creates modulated components with spatial frequencies at arbitrary multiples of $1/(\gamma G^s T)$, all along the direction $\hat{s}$ defined by the gradient pulses.

This immediately shows the value of the effective dipolar field (Eq. (7)). The actual dipolar field (from Eq. (6)) is strongly time dependent, becoming more modulated with time. The effective dipolar field is time independent and leads immediately to the full solution (which also must be the solution one would get from the actual dipolar field). The predicted magnetization can be nearly half the equilibrium

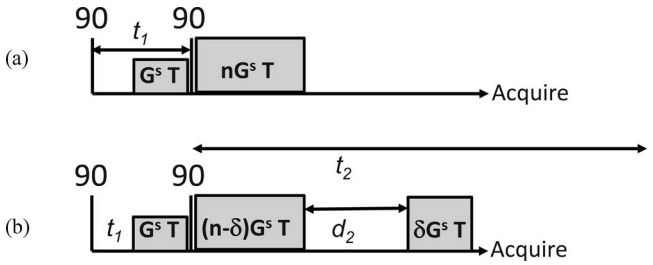

FIG. 2. The n-quantum CRAZED experiment produces signals in the indirectly detected dimension from intermolecular n-quantum coherences. (a) The traditional prototype sequence; (b) a sequence more reflective of common practice, since splitting the gradient reduces the bulk signal during d_2 and helps suppress radiation damping.

magnetization (and can be made even larger by replacing the second 90 pulse with a 120 pulse[24]).

In practice, the dipolar evolution competes with effects such as radiation damping and diffusion. As a result, the variant in Figure 2(b) is more common. According to Eqs. (7) and (9) splitting the gradient pulse makes no difference in the evolution by the end of the gradient pair, but it does eliminate the macroscopic magnetization for the period between the two gradient pulses, and thus reduces radiation damping effects.

Equation (13) predicts that the direction of the gradient pulse is quite important. For values of $t_2 \ll \tau_d$ (the most common case experimentally), an image created with x-gradient pulses should be almost exactly $-1/2$ of the image created with z-gradient pulses for a uniformly modulated sample, and the sum of x-, y-, and z-gradient images should vanish, thus reflecting only local anisotropy.

The effects of heteromolecular couplings can be dramatic. For example, the double-quantum CRAZED sequence (top of Figure 2 with $n = 2$) on a spherical sample of two components I and J (resonance frequencies ω_I and ω_J, respectively, here water and acetone) produces the spectrum in Figure 3. Homomolecular peaks appear at $(f_1 = 2\omega_I, f_2 = \omega_I)$ and $(f_1 = 2\omega_J, f_2 = \omega_J)$, and heteromolecular peaks appear at $(f_1 = \omega_I + \omega_J, f_2 = \omega_I)$ and $(f_1 = \omega_I + \omega_J, f_2 = \omega_J)$, reflecting apparent evolution at multiples of the resonance frequency in the indirectly detected dimension f_1, even though the Bloch equations predict no actual evolution at those frequencies during the first time interval. This disconnect is a consequence of nonlinear evolution in the modified Bloch equations. In contrast, the "coupled spin" picture uses the conventional density matrix equation of motion ($\dot{\rho} = i\hbar^{-1}[\rho, H]$) and makes the same set of assumptions about the retained part of the dipolar interaction (meaning that the Hamiltonian H has retained couplings proportional to $I_{zi}I_{zj}$). It shows that commonly neglected, higher order terms in the equilibrium density matrix leads to observable intermolecular multiple quantum coherences. In this case, the peak positions are readily understood. Intermolecular double quantum coherences evolve during the t_1 period; survive the double-quantum filter created by the mismatched gradient pulses; are partly converted into two-spin, one-quantum operators by the second pulse, and are made observable by commutation with the dipolar Hamiltonian.

Saving the signal from only the $f_1 = 2\omega_I$, $2\omega_J$, and $\omega_I + \omega_J$ peaks, the magnetization at the end of the sequence is

$$M_I^+(t_1,t_2) = M_{0,I}e^{i\omega_I t_2}\left\{\begin{array}{l} e^{-i2\omega_I t_1}2\left(\frac{\tau_{d,I}}{\Delta\ t_2}\right)J_2\left(\frac{\Delta\ t_2}{\tau_{d,I}}\right)J_0\left(\frac{2\Delta\ t_2}{3\tau_{d,J}}\right) \\ +e^{-i(\omega_I+\omega_S)t_1}\left(\frac{\tau_{d,I}}{\Delta\ t_2}\right)J_1\left(\frac{\Delta\ t_2}{\tau_{d,I}}\right)J_1\left(\frac{2\Delta\ t_2}{3\tau_{d,J}}\right)\end{array}\right\}$$
$$M_J^+(t_1,t_2) = M_{0,J}e^{i\omega_J t_2}\left\{\begin{array}{l} e^{-i2\omega_J t_1}2\left(\frac{\tau_{d,J}}{\Delta\ t_2}\right)J_2\left(\frac{\Delta\ t_2}{\tau_{d,S}}\right)J_0\left(\frac{2\Delta\ t_2}{3\tau_{d,I}}\right) \\ +e^{-i(\omega_I+\omega_J)t_1}\left(\frac{\tau_{d,J}}{\Delta\ t_2}\right)J_1\left(\frac{\Delta\ t_2}{\tau_{d,J}}\right)J_1\left(\frac{2\Delta\ t_2}{3\tau_{d,I}}\right)\end{array}\right\} \quad (14)$$

For short values of t_2 the signals for the homomolecular peaks are proportional to $M_{0,I}^2\ \Delta\ t_2$ and $M_{0,J}^2\ \Delta\ t_2$, and the heteromolecular peaks are each proportional to $2M_{0,J}M_{0,I}\Delta\ t_2/3$. In very concentrated solutions, higher order double-quantum peaks such as $(f_1 = 3\omega_I - \omega_J, f_2 = \omega_I)$ can also be observed. Both the mean-field and the coupled-spin pictures make the same predictions; the mean-field is easier to use for numerical simulations, but the coupled-spin picture makes the physical evolution much more transparent, and is more useful for pulse sequence design.

We should also note that the derivation of Eq. (6) shows immediately that the modulation can be more complex than a single sine wave, as long as all the spatial components have the same value of Δ; for example, the ZEBRA sequence[25] alternates stripes of fully inverted and uninverted magnetization, and is also analytically solvable.

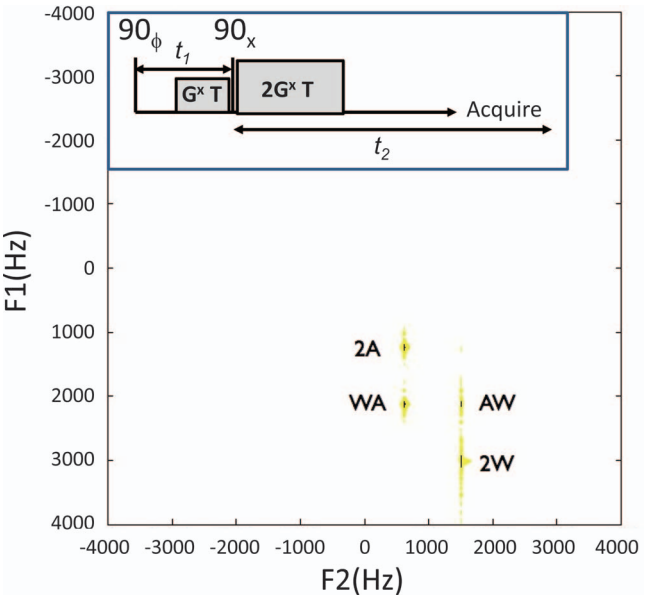

FIG. 3. Double-quantum CRAZED pulse sequence, which produces signals from intermolecular multiple-quantum coherences as described in text. The two gradient pulses (shaded boxes) are configured in a 1:2 area ratio, which suppresses all conventional signals. This experimental data comes from a tube with equal volumes of acetone and water, with resonance offsets 630 Hz and 1500 Hz, respectively; all gradient pulses were 1.5 ms duration.

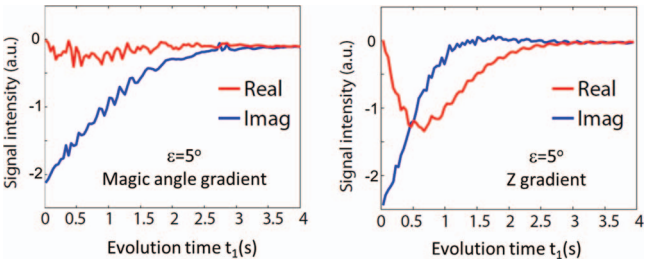

FIG. 4. Experimental signals from the sequence in Figure 1(b), for magic angle (left) or z gradient (right). The magic angle gradients generated an unshifted signal.

III. PROBLEMS WITH THE CONVENTIONAL FRAMEWORK

A. Gradient pulse pairs

As it turns out, astonishingly simple experiments disagree significantly with the mathematical framework in Eqs. (7) and (9). Consider the simple pulse sequence in Figure 1(a), applied for simplicity to a spherical sample. The first pulse flip angle is chosen to be extremely small, so that almost all of the magnetization remains along the z-axis, and thus produces no dipolar field. Thus, the firm prediction is that the magnetization evolution frequency reflects no dipolar field effects, and certainly is independent of the direction of the gradient. In fact, such matched gradient pairs are a very common module in pulse sequence design, which have become even more important with the advent of hyperpolarization technologies;[26] in hyperpolarized imaging, generally the sample magnetization is used to create multiple images by restricting pulses to small flip angles.

Figure 1(b) presents a variant which is easier to test (since there are no residual radiation damping or inhomogeneous broadening effects, but dipolar effects are not affected by an echo pulse). Figure 4 demonstrates this sequence experimentally with $\varepsilon = 5^\circ = 0.087$ rad on a spherical water sample at 7T($\tau_d = 130$ ms). When the small magnetization is modulated at the magic angle the decay is indeed completely controlled by T_2. For z-modulation there is an *experimentally measured shift*. Replacing the initial 5° pulse with a 175° pulse experimentally reverses the direction of the frequency shift. As we discuss later, in our corrected framework, this happens because the transverse magnetization produces a very small dipolar field whose effects are greatly magnified by the (seemingly innocuous) large bulk magnetization, even though that magnetization by itself produces no dipolar field. In fact, this shift would persist in the limit of an *arbitrarily small rf pulse* (at least down to the limit where statistical fluctuations in the magnetization density dominate).

The two-dimensional experiments we will use to illustrate the problems with the conventional framework are the multi-axis CRAZED or MAX-CRAZED (Fig. 1(c)) and GRACE (gradient-embedded COSY experiment, Fig. 1(d)). MAX-CRAZED experiments simply add a strong balanced gradient pair with separation d_2 to a CRAZED sequence, along a direction s' different from the correlation gradient direction. Only the transverse magnetization is affected by these gradient pulses, not the z axis modulation. Thus, Eqs. (7) and (9) predict that diffusional attenuation of the detected single-quantum coherences should be the only difference between the MAX-CRAZED and CRAZED. Table I and Figures 5 and 6 focus on two specific cases: in both cases the correlation gradients s are along x, and the additional gradients s' are along y and z in the XY MAX-CRAZED and XZ MAX-CRAZED, respectively. The two MAX-CRAZED experiments are arranged to have precisely the same diffusional weighting at all times, and $G^{s'} = 10\ G^{s}$.

In fact, Table I shows the XY MAX-CRAZED does not alter the ratio of peak heights, but the XZ combination dramatically suppresses homomolecular peaks. To explore this further, we varied the delay d_2 between the gradient pulses in the interval after the second rf pulse, keeping the total time before signal acquisition fixed at 60 ms. As Figure 5 shows that the XZ-MAXCRAZED differs

TABLE I. Comparison of the four peak intensities in the CRAZED and MAX-CRAZED experiments, here with $d_2 = 60$ ms. The "absolute" numbers give intensities relative to the strongest X-CRAZED; the "normalized" numbers in parentheses are intensities with the homomolecular water peak given intensity 1 in each spectrum.

Peak (f_1, f_2)	Expected intensity	X-CRAZED	XY-MAXCRAZED absolute (normalized)	XZ-MAXCRAZED absolute (normalized)
(2W, W)	1.00	1.00	0.23 (1.00)	0.07 (1.00)
(A+W, W)	0.46	0.44	0.11 (0.46)	0.12 (1.79)
(A+W, A)	0.46	0.51	0.15 (0.67)	0.18 (2.60)
(2A, A)	0.48	0.48	0.14 (0.66)	0.04 (0.64)
Hetero/homo	**0.62**	**0.64**	**0.68**	**2.65**

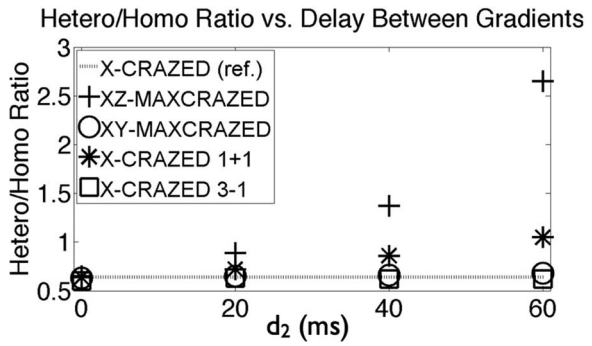

FIG. 5. Ratios of the heteromolecular (f_1 at the sum of the acetone and water frequencies) to the homomolecular peaks for various MAXCRAZED sequences, as a function of the delay between the gradient pulses. In the conventional treatment, this should affect nothing except a possible diffusion weighting. In fact, for the XZ-MAXCRAZED it drastically alters peak intensity, and it modestly alters peak intensity for the 1+1 X-CRAZED.

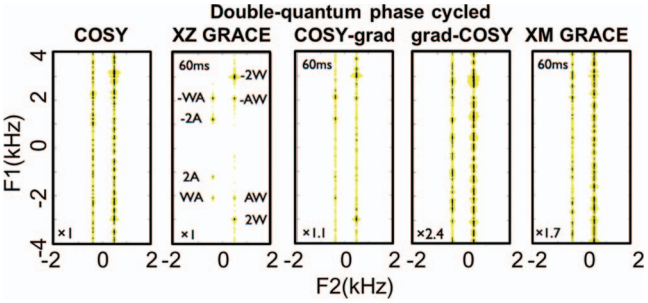

FIG. 7. Experimental data for the sequences in Figure 5, applied to a spherical sample of acetone in water. The sample was an 8 mm sphere with equal volumes of acetone and water, studied in a 360 MHz NMR spectrometer with a 25 mm microimaging coil (giving a small filling factor and the modest radiation damping effects). The phase cycled COSY only gives residual t_1 noise, as expected, as does the grad-COSY combination and the XM GRACE; the XZ GRACE and COSY-grad experiments show double-quantum peaks.

dramatically from the other sequences for all delay values. The only other, much smaller, difference is with the 1+1 CRAZED ($\delta = 1$ in Figure 2(b)), which we will discuss later; the 3-1 CRAZED ($\delta = -1$ in Figure 2(b)) looks like the conventional sequence.

Figure 6 compares the peak intensities for the XZ and XY MAXCRAZED experiments to a simple prediction based on diffusion weighting; since virtually all of the diffusional effects take place in the final time interval, and the transverse magnetization is much more highly modulated than is the z magnetization, the peaks are expected to be attenuated according to the conventional (single-quantum) diffusion weighting of the detected spin. Figure 6 shows that this prediction accurately gives the signal strengths for all peaks in the XY MAXCRAZED, and for all of the heteromolecular peaks in the XZ MAXCRAZED experiment, but *not* the homomolecular peaks, which are strongly attenuated.

The situation is even more bizarre in the GRACE experiment (Figure 1(d)), which is basically a COSY with matched gradient pulse pairs in the two time domains. To highlight any possible (unexpected) double-quantum signal, we perform double-quantum phase cycling on the first pulse (coadding spectra with first pulse phase 0 and 180, subtracting spectra

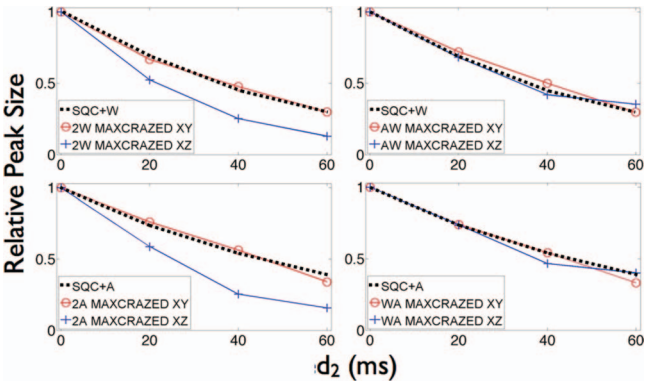

FIG. 6. Comparison of the observed signal in the MAXCRAZED experiments from the predictions by simple diffusion weighting (dashed lines). The XZ MAXCRAZED deviates dramatically from those predictions, but only for the homomolecular peaks (left).

with first pulse phase 90 and 270). Experimentally, we focus on the XZ-GRACE and XM-GRACE, where the second set of gradient pulses is along z or the magic angle, respectively. We compare this to what we will call COSY-grad (the gradient pair in t_1 omitted) and grad-COSY (the gradient pair in d_2 omitted). The longitudinal magnetization is zero during t_1 and kept unmodulated during d_2. Thus, there should be no modulated-magnetization contribution to dipolar field effects, and if we choose a spherical sample, there should be no dipolar effects from any average magnetization. Hence a double-quantum phase cycled GRACE spectrum should show no peaks (except perhaps for residual single or zero quantum coherence by imperfect phase cycling). However, Figures 7–9 show that the conventional picture fails again here. The GRACE spectrum, with gradient pulses along Z in the second interval, shows strong water-water and acetone-acetone peaks, but weak water-acetone peaks. Only residual t_1 noise is visible in the COSY spectrum, the grad-COSY spectrum, or the XM-GRACE. The COSY-grad and XZ-GRACE produce double-quantum peaks, which are noisy but readily seen by varying the delay d_2 (Figures 8 and 9).

The peaks in the GRACE experiment are much weaker than the conventional peaks, which is the reason the t_1 noise is so prominent. We do not suspect the GRACE experiment is particularly practical (as opposed to the different CRAZED variants, which have numerous applications) but they do serve to illustrate a problem with the conventional treatment, even when the z magnetization is completely unmodulated during the final time interval. In addition, the difference between the XZ-GRACE and XM-GRACE is a strong clue that the explanation somehow lies in dipolar effects, since nothing else would be affected by the choice of gradient direction in a spherical sample.

IV. REVISED FRAMEWORK FOR DIPOLAR EFFECTS

It has long been recognized[27] that there is a limitation in the framework that leads to Eqs. (7) and (9), which is that is that it was derived for uniformly modulated magnetization (although at least one recent paper seems to have incorrectly ignored this limitation[28]). This means that the basic

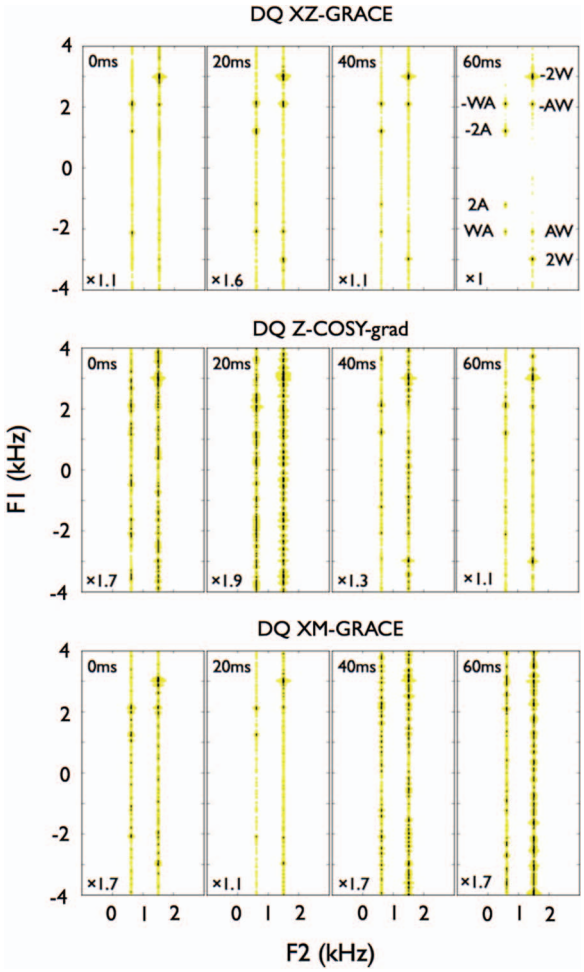

FIG. 8. Comparison of observed spectra as a function of the delay between the two strong gradients d_2, which is the interval when the transverse magnetization is modulated. The XZ-GRACE, and to a lesser extent the COSY-grad experiment, show growth of DQ peaks; the XM-GRACE does not.

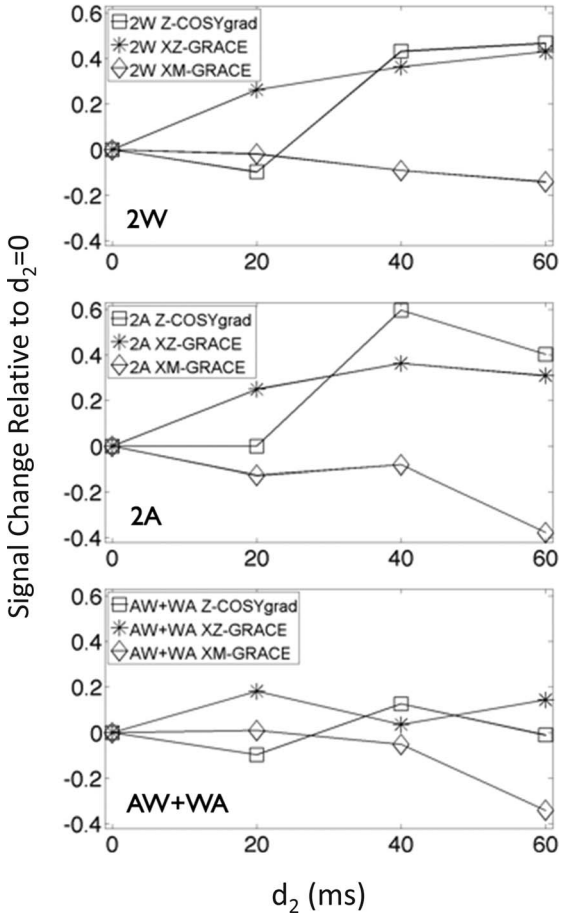

FIG. 9. Comparison of the homomolecular and heteromolecular peak intensities for the GRACE and COSY-grad experiments, as a function of the delay between the gradient pulses. Homomolecular peak intensities grow with increasing delay in the XZ-GRACE and COSY-GRAD experiments, heteromolecular intensities do not.

underlying assumption in going from Eqs. (5) to (6) is violated *whenever there is a signal* (this would imply the component at $\vec{k} = 0$ does not vanish, which causes a problem with the singularity at $\vec{k} = 0$ in Eq. (5)). The sequences in Figure 1(a), 1(b), and 1(d) violate this assumption by leaving behind bulk magnetization, and even though that magnetization is in a spherical sample (and hence produces no dipolar field) it clearly has some measurable effect. Reference 27 argued that the expressions for the effective dipolar field in Eqs. (7) and (9) can be corrected by subtracting the average of each magnetization component for a spherical sample (since the average magnetization would induce no dipolar field).

$$\begin{aligned}
\vec{B}_d(\vec{r}) &= \mu_0\Delta[2(M_z(\vec{r}) - \langle M_z\rangle)\hat{z} - (M_x(\vec{r}) \\
&\quad - \langle M_x\rangle)\hat{x} - (M_y(\vec{r}) - \langle M_y\rangle)\hat{y}]/3, \\
\vec{B}_{d,eff}(\vec{r}) &= \mu_0\Delta\ M_z(\vec{r})\hat{z} + [-2\langle M_z\rangle\hat{z} \\
&\quad + \langle M_x\rangle\hat{x} + \langle M_y\rangle\hat{y}]/3 \quad \text{(homomolecular)}, \\
\vec{B}_{d,eff}(\vec{r}) &= \mu_0\Delta[2(M_z(\vec{r}) - \langle M_z\rangle)\hat{z}]/3 \quad \text{(heteromolecular)}.
\end{aligned} \tag{15}$$

This is the effect which dominates the unexpected behavior for the gradient sequence in Figure 4 and the GRACE experiments. The appearance of average magnetization terms in Eq. (15) spoils the exact solution of the CRAZED sequence in Figure 2(a), Eq. (13). However, so does relaxation, diffusion and radiation damping, so the disagreement between the exact theory and experiment has not been considered serious; the insight for pulse sequence design is unaffected. Note, however, that it does not spoil the solution for the sequence with the split gradient pulses (Figure 2(b)); as long as δ is not an integer, no transverse magnetization exists during the time d_2 so the signal after the final gradient pulse exactly matches Eq. (13).

The XZ combination of MAX-CRAZED (Figure 1(c)) violates this assumption in a different way, by modulating longitudinal and transverse magnetization along axes with different values of Δ. These sequences were chosen to produce particularly clear disagreement between theory and experiment, but the problem is more general. Gradient pulse pairs are a seemingly innocuous module in thousands of pulse sequences. Small flip angle pulse images (with large amounts of residual magnetization) are ubiquitous in hyperpolarized imaging, one of the most rapidly growing fields of magnetic resonance. More generally, imaging components in a pulse

sequence, such as read and phase encode gradients, only modulate the transverse components of the magnetization, so in virtually every imaging experiment the assumption of a unique direction to the modulation is unwarranted.

Understanding these effects requires a more careful reconsideration of the assumptions leading to Eqs. (7) and (9), and a reformulation of the problem. To be clear, rolling back the clock almost four decades, and working only from Eq. (4) (the nonlocal form of the dipolar field) would correctly describe the results of all of these experiments-but that is not a practical solution. We do not believe anyone would have *expected* these results from that approach, let alone predict how these differences would affect other modern sequences (particularly because some of the sequences in Figure 1 are not related to traditional dipolar field experiments). To the extent that there is a general intuition about dipolar field effects, it is that modulated magnetization produces a dipolar field of order $\gamma\mu_0$ times that magnetization-yet the frequency shift in Figure 4 is an order of magnitude larger than that prediction. This paper will focus on simple corrections to the existing framework which do predict the observed effects.

To make this concrete, let us assume a spherical sample of radius R, with each of the x, y, and z components of the magnetization decomposed into two parts:

- a sphere with uniform magnetization $\langle\vec{M}\rangle = \langle M_x\rangle\hat{x} + \langle M_y\rangle\hat{y} + \langle M_z\rangle\hat{z}$. This uniform magnetization produces no dipolar field (inside the sphere), no matter the direction of $\langle\vec{M}\rangle$.
- residual x, y, and z components (e.g., $(M_x(\vec{r}) - \langle M_x\rangle)\hat{x}$) inside the sample which might have multiple spatial frequencies and modulation directions, e.g.,

$$M_x\left(k_x^x, k_x^y, k_x^z\right) = \int_{sphere} (M_x(x, y, z) - \langle M_x\rangle) \times e^{i(k_x^x x + k_x^y y + k_x^z z)} dx\, dy\, dz \quad (16)$$

with analogous equations for $M_y(k_y^x, k_y^y, k_y^z)$ and $M_z(k_z^x, k_z^y, k_z^z)$. Thus in our notation, the wavevectors k are labeled with a subscript that is a spin direction, and a superscript that is a spatial variable.

The x, y, and z magnetizations can be modulated in different directions. However, in what follows, we assume that all of the nonvanishing components of $M_x(k_x^x, k_x^y, k_x^z)$ have the same value of $\Delta_x = (3((k_x^z)^2/((k_x^x)^2 + (k_x^y)^2 + (k_x^z)^2)) - 1)/2$ (with analogous equations for the y and z components, possibly with different values of Δ_y and Δ_z). We will also assume that the wavevectors of the nonvanishing components are always $\gg 1/R$ (this is equivalent to assuming that the "modulated component" is in fact highly modulated across the sample).

Note that this is *not* the same as saying that the magnetization only has a $k = 0$ component and highly modulated components, as the sphere itself creates a range of spatial Fourier components. The Fourier transform of a sphere of radius R ($p(R)$) is also spherical, with amplitude given by

$$W(\vec{k}, R) = \int p(\vec{r}) \exp(2\pi i(\vec{k} \bullet \vec{r}))d\vec{r} = R^3 \frac{2\pi^{3/2}}{\Gamma(3/2)(2\pi|\vec{k}|R)^2} \left[\frac{\sin(2\pi|\vec{k}|R)}{(2\pi|\vec{k}|R)} - \cos(2\pi|\vec{k}|R)\right] \quad (17)$$

This approach correctly resolves the singularity present in Eq. (5) at the origin $k = 0$, by subtracting a set of spatial components proportional to Eq. (17) in a way that nulls out the $k = 0$ component without distorting the dipolar field. Thus by construction the magnetization components with $k_x^x = k_x^y = k_x^z = 0$, $k_y^x = k_y^y = k_y^z = 0$, or $k_z^x = k_z^y = k_z^z = 0$ all vanish.

Now the three vector components of Eq. (5) should be treated separately. The effects of the modulated and unmodulated components can also be separated because Eq. (5) is linear in the magnetization. The uniform spherical components produce no dipolar field. The modulated components produce different dipolar fields because of the different directions, but under the assumption above it is straightforward to show that

$$\vec{B}_d(\vec{r}) = \frac{\mu_0}{3}[2\Delta_z(M_z(\vec{r}) - \langle M_z\rangle)\hat{z} - \Delta_x(M_x(\vec{r}) - \langle M_x\rangle)\hat{x} - \Delta_y(M_y(\vec{r}) - \langle M_y\rangle)\hat{y}] \text{ (homomolecular).} \quad (18)$$

It is trivial to generalize this result to other shapes with known analytic solutions (ellipsoidal samples). We note, however, that even for these simple shapes modulated by a perfect gradient pulse, the dipolar field does not exactly track the magnetization; it is different at the edges than at the center. Even a spherical sample with highly modulated magnetization will have high Fourier components, representing the edges of the sphere. As a result, within about $1/k$ of the edges, the numerical factor $(3(\hat{k} \bullet \hat{z})^2 - 1)/2$in the first brackets of Eq. (5) is not identical for all of the spatial frequency components. For example, a z-modulated sphere will tend to lose high frequency components in the x and y directions, making the dipolar field more fall off more in those directions. These complications are important for a quantitative analysis, for example in imaging experiments which measure anisotropy by comparing images with X-, Y-, and Z- gradients, and will be treated in a later paper. However, they are not important for explaining the experiments described here. What this implies is that when bulk magnetization forms, even in a spherical sample, it forms in a pattern that is not perfectly spherical.

Equation (18) reduces to Eq. (6) when the magnetization is fully modulated in a single direction, but leaving it in this form reveals some remarkable physics. It is possible to create sequences with the x and y components modulated in different directions (for example, 90_x-{z gradient}-45_x-{x+y gradient}-90_y, with spins on resonance, would create $\Delta_z = \Delta_y = 0$ and $\Delta_x = 1$). This converts Eq. (18) into $\vec{B}_d(\vec{r}) = -(\mu_0/3)(M_x(\vec{r})\hat{x})$. But recall that the secular

approximation was already made, in going from Eqs. (3) to (4). We thus produce *a secular Hamiltonian proportional to* I_x!

How can a secular Hamiltonian have that form (which we would normally associate with the rotations made by a rf pulse, which is obviously nonsecular)? It is straightforward to show from Eq. (4) that[29]

$$d\langle M_z\rangle/dt = \int d^3\vec{r}\ (d\vec{M}(\vec{r})/dt)_z = \int d^3\vec{r}\ (\gamma\vec{M}(\vec{r}) \times B_d(\vec{r}))_z = 0. \quad (19)$$

In other words, the bulk z magnetization (hence the energy) is not changed by the interaction of the spins with the dipolar field. Thus, even though the dipolar Hamiltonian rotates spins along the x axis and thus changes the *local* z magnetization, every position where the z magnetization is made more positive is counterbalanced by one which makes it more negative. Energy is transported within the sample (over macroscopic distances corresponding to $1/|\vec{k}|$) but not outside of it.

For the MAXCRAZED experiments (and, indeed, for the vast majority of magnetic resonance applications, including imaging applications) the two transverse magnetization components have the same modulation direction, $\Delta_x = \Delta_y = \Delta_\perp$. We can then rewrite Eq. (16) and simplify to an effective field by adding $\mu_0\Delta_\perp\vec{M}/3$:

$$\vec{B}_d(\vec{r}) = \frac{\mu_0}{3}[2\Delta_z(M_z(\vec{r}) - \langle M_z\rangle)\hat{z} - \Delta_\perp((M_x(\vec{r}) - \langle M_x\rangle)\hat{x} + (M_y(\vec{r}) - \langle M_y\rangle))\hat{y}] \quad \text{(homomolecular)},$$
$$\vec{B}_{d,eff}(\vec{r}) = \frac{\mu_0}{3}[(2\Delta_z + \Delta_\perp)M_z(\vec{r})\hat{z} + (\Delta_\perp\langle M_x\rangle\hat{x} + \Delta_\perp\langle M_y\rangle\hat{y} - 2\Delta_z\langle M_z\rangle\hat{z})] \quad \text{(homomolecular)}. \quad (20)$$

The heteromolecular case proceeds similarly to the homomolecular case, except that only the z component is retained in Eq. (18):

$$\vec{B}_{d,eff}(\vec{r}) = \frac{\mu_0}{3}(2\Delta_z(M_z(\vec{r}) - \langle M_z\rangle)\hat{z} \quad \text{(heteromolecular)}. \quad (21)$$

Equations (20) and (21) are the correct replacements for Eqs. (7) and (9). Equation (21) is equivalent to the result produced in Ref. 27 (and Eq. (15)), but Eq. (20) is very different from the results there, and it is the homomolecular case where the changes are most profound.

For the matched-gradient pair sequences in Figures 1(a), 1(b), and 4, the first pulse flip angle is chosen to be extremely small, so that almost all of the magnetization remains along the z-axis and produces no dipolar field. Equation (20) simplifies to

$$\vec{B}_d(\vec{r}) = \frac{\mu_0}{3}[-\Delta_\perp((M_x(\vec{r})\hat{x} + M_y(\vec{r})\hat{y}))];$$
$$\gamma|\vec{B}_d(\vec{r})| = \varepsilon\,\gamma\,\mu_0 M_0\Delta_\perp/3 = \varepsilon\,\Delta_\perp/3\tau_d$$
$$\vec{B}_{d,eff}(\vec{r}) = \frac{\mu_0}{3}[\Delta_\perp M_z(\vec{r})\hat{z}];$$
$$\gamma|\vec{B}_{d,eff}(\vec{r})| = \gamma\,\mu_0 M_0\Delta_\perp/3 = \Delta_\perp/3\tau_d. \quad (22)$$

The actual dipolar field is very small, and proportional to the small pulse flip angle ε. However, the effective dipolar field is *much larger* and *independent of* ε-it gives a dipolar frequency shift from the full magnetization. The origin of this nonintuitive result is simple: the dipolar field from the slightly modulated magnetization is an xy-field, and hence affects the large z magnetization. Only converting it to an *effective* field along the z axis reveals the true significance.

For z-modulation ($\Delta_\perp = 1$), the actual dipolar field in Figure 4 (in frequency units) from Eq. (22) would be 0.22 rad s^{-1}, but the effective dipolar field would be 2.5 rad s^{-1}, close to the experimentally measured shift. Replacing the initial 5° pulse with a 175° pulse experimentally reverses the direction of the frequency shift, as expected.

Thus, modulating a trivially small amount ε of the magnetization alters the apparent resonance frequency by an amount independent of ε, although eventually very small flip angles would cause magnetization fluctuations to be important, and those are ignored here. These effects would of course be larger at higher fields or with a hyperpolarized sample, and unlike radiation damping effects are not reduced by "water flipback" pulses that keep the magnetization near equilibrium. This result has potential substantial consequences for hyperpolarized experiments, where images are commonly acquired by modulating a tiny fraction of the magnetization at a time. In addition, even couplings between unlike spins revert to the homomolecular case under a multiple echo sequence or spin locking, so (for example) water can certainly affect the magnetization of another molecule under those circumstances.

For the GRACE experiment, during d_2 the z-magnetization is unmodulated, but its value depends explicitly on the evolution time t_1:

$$M_z = -M_{0,I}\cos(\omega_I t_1) - M_{0,J}\cos(\omega_J t_1) \quad (23)$$

The x- and y-components are fully modulated, giving

$$\vec{B}_{d,eff}(\vec{r}) = -\frac{\mu_0}{3}(\Delta_\perp\langle M_z\rangle)\hat{z} \quad \text{(homomolecular)};$$
$$\vec{B}_{d,eff}(\vec{r}) = 0 \quad \text{(heteromolecular)}. \quad (24)$$

Even though the unmodulated magnetization, by itself, generates no dipolar field, the combination of modulated and unmodulated magnetization creates an effective dipolar field proportional to the unmodulated magnetization. Thus the XZ-GRACE experiment (with ($\Delta_\perp = 1$)) creates homomolecular peaks which grow during d_2; the XM-GRACE experiment, with $\Delta_\perp = 0$, does not. In both cases normal evolution resumes during t_2.

We now turn to the MAXCRAZED sequences. *If* Eqs. (20) and (21) are valid and the average magnetization is small, the dipolar field is

$$\vec{B}_{d,eff}(\vec{r}) = \frac{\mu_0}{3}(2\Delta_z + \Delta_\perp)M_z(\vec{r})\hat{z} \quad \text{(homomolecular)},$$
$$\vec{B}_{d,eff}(\vec{r}) = \frac{\mu_0}{3}(2\Delta_z)M_z(\vec{r})\hat{z} \quad \text{(heteromolecular)}. \quad (25)$$

The question is the validity of Eqs. (20) and (21). At the beginning of the interval d_2, the transverse magnetization is modulated with two spatial frequencies, $\gamma((n+1)G^sT\hat{s} + G^{s'}T\hat{s}')$ and $\gamma\,((n-1)G^sT\hat{s} + \gamma G^{s'}T\hat{s}')$

which in the general case will be along two different directions with different values of Δ, and thus will make Eqs. (20) and (21) invalid. Fortunately, in the XY MAXCRAZED experiment ($\hat{s} = \hat{x}$, $\hat{s}' = \hat{y}$) the value of Δ for both of these components is the same ($-1/2$) so Eqs. (20) and (21) hold. We then have $\Delta_z = \Delta_\perp = -1/2$, and the homomolecular coupling is 1.5 times greater than the homomolecular, just as in CRAZED. The full solution for double-quantum XY MAXCRAZED during d_2 is a simple generalization of Eqs. (11) and (12):

$$\begin{aligned} M^+ &= e^{i\omega d_2} e^{i2\gamma G^s T s} e^{i\gamma G^{s'} T s'} \exp\{i(-1/2)\gamma\,\mu_0 M_z d_2\} \\ &\quad \times i M_0 \sin(\omega t_1 + \gamma G^s T s) \\ &= e^{i\omega d_2} e^{i2\gamma G_s T s} e^{i\gamma G_{s'} T s'} \exp\{(i/2)\gamma\,\mu_0 M_0 d_2 \\ &\quad \times \cos(\omega t_1 + \gamma G^s T s)\} i M_0 \sin(\omega t_1 + \gamma G^s T s) \\ &= e^{i\omega d_2} e^{i2\gamma G^s T s} e^{i\gamma G^{s'} T s'} i M_0 \sin(\omega t_1 + \gamma G^s T s) \\ &\quad \times \sum_{m=-\infty}^{\infty} i^m J_m(d_2/2\tau_d) e^{im\omega t_1 + im\gamma G^s T s} \\ &= e^{i\omega d_2} M_0 \left(\sum_{m=-\infty}^{\infty} i^{m+1} (m(-2\tau_d/d_2) J_m(-d_2/2\tau_d)) \right. \\ &\quad \left. \times [e^{im\omega t_1 + i(2+m)\gamma G^s T s + i\gamma G^{s'} T s'}] \right). \end{aligned} \tag{26}$$

The final gradient pulse unwinds the s' modulation and gives a signal identical to Eq. (13) with $\Delta = -1/2$, in agreement with experiment. Note that the transverse magnetization becomes very complex with time (the directions of the frequency components actually change, as new spatial frequencies are created in the xy plane, as opposed to the case in Eq. (12)) but since all of these components would give $\Delta = -1/2$, they do not alter the conclusion that Eq. (25) is valid. In fact, any combination where $\hat{s}$ and $\hat{s}'$ are both in the xy plane (even if they are not orthogonal) is solvable, as long as $aG^s\hat{s} + bG^{s'}\hat{s}' \neq 0$ for integer a and b (otherwise, some terms in the final bracket of Eq. (26) will be unmodulated); and in the practical limit, only very small integer values of a and b are important.

Another case that is generally solvable is the limit $G^{s'}T \gg G^sT$, since then the two modulation components have (nearly) the same value of Δ. Thus, the magnetization at the beginning of d_2 does satisfy the assumptions behind Eq. (25), and the short time behavior would be described by those relations. In fact, in the X-Z MAXCRAZED experiment in that limit, both of the spatial frequencies for the transverse magnetization have $\Delta_\perp = 1$, and the homomolecular dipolar coupling *vanishes* during the delay d_2 since $\Delta_z = -1/2$ and $\Delta_\perp = 1$. *The mixed gradient pulse direction effectively performs homomolecular decoupling*-leaving only the heteromolecular peaks in the two-dimensional spectrum.

For other pairs of gradient directions, the evolution creates new Fourier components in directions which add multiples of $G^sT\hat{s}$. In that case the dipolar field eventually becomes nonlocal even if $\Delta_s = \Delta_{s'}$, since even in that limit Δ for the sum of the two vectors can be different from Δ for the vectors themselves (for example, the sum of two magic angle gradients need not be at the magic angle). However, in most practical applications only the short time behavior ($d_2/\tau_d < 1$) matters, and Eq. (25) retain predictive power.

The only other case that is analytically solvable in general is the case $\hat{s} = \hat{s}'$. In Figure 5 the 3-1 CRAZED experiment ($\hat{s} = \hat{s}' = \hat{z}$, $G^s = G^{s'}$) looks like the normal CRAZED, because while we have changed the k vectors of the modulated transverse magnetization during the delay between the pulses, the direction is unchanged and the dipolar field still looks proportional to the local magnetization. During the interval d_2 the sequence looks like a triple-quantum CRAZED, and the signal is small enough to be ignored. The 1+1 CRAZED experiment ($\hat{s} = \hat{s}' = \hat{z}$, $G^s = -G^{s'}$) on the other hand, creates a partial echo which reintroduces some radiation damping effects and alters the homomolecular dipolar field.

V. DISCUSSION AND CONCLUSIONS

We have shown that the mathematical picture which underpins the mean-field picture of dipolar field effects relies on some significant oversimplifications. When this picture was originally proposed, to deal with multiple echoes in ^{3}He, the approximation that everything was modulated in the same direction was appropriate, although even then it could be argued that ignoring the effects of the echoes themselves (which create bulk magnetization) was incorrect. The real issue, however, is that experimental applications have evolved, in directions which could scarcely have been imagined when multiple echoes were first observed; and the mean-field framework has never been seriously re-examined to reflect the new experimental conditions.

The results presented here do not invalidate the decades of published work on intermolecular multiple-quantum coherence effects-just as recognition of those effects did not invalidate decades of work on two-dimensional NMR, where they had been ignored-but they do have some significant consequences. Recognizing the limitations in the original derivations (which, to be fair, were stated clearly in the original papers) predicts pulse sequences with highly unexpected effects, such as the MAXCRAZED and GRACE experiments here. The GRACE experiments are mostly interesting from a pedagogical perspective, because the signals are small; the MAXCRAZED sequences, on the other hand, provide a new method for suppressing homomolecular coherences which might be quite useful. For example, in temperature imaging[16] or brown adipose tissue detection[30] the interesting information is contained entirely in the water-fat heteromolecular coherences and the water-water or fat-fat peak provide a background to be suppressed.

This work also challenges some longstanding beliefs in magnetic resonance. We have shown it is possible to have a secular Hamiltonian proportional to I_x. We have shown that it is possible to see dipolar effects from the interior of uniformly modulated, spherical magnetization. We have shown that a seemingly innocuous module in *thousands* of existing pulse sequences (matched gradient pulse pairs) can actually alter the time evolution other than by simple diffusion, and may be broadly important. In the end, almost all of the analytical

DDF expressions are wrong, even ignoring radiation damping, diffusion and relaxation, and they do not appear to be amenable to simple analytical solutions (although numerical integration remains straightforward). Finally, our results show that iMQC methods to image anisotropy need to be re-evaluated to produce quantitative results; in general, the phase-encode and readout gradients needed to produce an image alter the DDF, by an amount which depends on the correlation gradient direction.

ACKNOWLEDGMENTS

This work was supported by the National of Institutes of Health (NIH) under Grant No. EB02122. We wish to thank Richard Bowtell for stimulating and useful discussions on the secular approximation in this problem. We also wish to thank Jean Jeener for his extraordinary efforts in helping to refine and clarify the arguments in this paper. His insight is greatly valued.

[1] J. H. van Vleck, Phys. Rev. **74**, 1168–1183 (1948).
[2] A. Abragam, *The Principles of Nuclear Magnetism* (Clarendon, Oxford, 1961), Chap. 3.
[3] A. K. Khitrin, V. L. Ermakov, and B. M. Fung, Chem. Phys. Lett. **360**, 161 (2002); A. K. Khitrin, J. Chem. Phys. **134**, 154502 (2011).
[4] S. W. Morgan, B. V. Fine, and B. Saam, Phys. Rev. Lett. **101**, 067601 (2008).
[5] N. Bloembergen, E. Purcell, and R. V. Pound, Phys. Rev. **73**, 679 (1948).
[6] G. Deville, M. Bernier, and J. M. Delrieux, Phys. Rev. B **19**, 5666 (1979).
[7] H. T. Edzes, J. Magn. Reson., **86**, 293 (1990).
[8] R. Bowtell, J. Magn. Reson. **100**, 1 (1992).
[9] W. S. Warren, W. Richter, A. H. Andreotti, and B. T. Farmer II, Science **262**, 2005 (1993).
[10] W. S. Warren, "Concentrated solution effects," in *Encyclopedia of Magnetic Resonance* (Wiley, 2011).
[11] L.-S. Bouchard and W. S. Warren, J. Magn. Reson. **177**, 9 (2005).
[12] R. T. Branca, Y. M. Chen, V. Mouraviev, G. Galiana, E. R. Jenista, C. Kumar, C. Leuschner, and W. S. Warren, Magn. Reson. Med. **61**, 937–943 (2009).
[13] D. Z. Balla and C. Faber, J. Chem. Phys. **128**, 154522 (2008).
[14] S. Vathyam, S. Lee, and W. S. Warren, Science **272**, 92–96 (1996); Y.-Y. Lin, S. Ahn, N. Murali, W. Brey, C. R. Bowers, and W. S. Warren, Phys. Rev. Lett. **85**, 3732 (2000).
[15] Z. Chen, Z. Chen, and J. Zhong, J. Am. Chem. Soc. **126**, 446 (2004).
[16] G. Galiana, R. T. Branca, E. R. Jenista, and W. S. Warren, Science **322**, 421–424 (2008).
[17] S. Lee, W. Richter, S. Vathyam, and W. S. Warren, J. Chem. Phys. **105**, 874–900 (1996).
[18] J. Jeener, A. Vlassenbroek, and P. Broekaert, J. Chem. Phys. **103**, 1309 (1995).
[19] W. S. Warren and S. Ahn, J. Chem. Phys. **108**, 1313 (1998).
[20] A. Vlassenbroek, J. Jeener, and P. Broekaert, J. Magn. Reson., Ser. A **118**, 234 (1996); M. H. Levitt, Concepts Magn. Reson. **8**, 77 (1996).
[21] J. Jeener, J. Chem. Phys. **116**, 8439 (2002).
[22] Y. Y. Lin, N. Lisitza, S. Ahn, and W. S. Warren, Science **290**, 118 (2000).
[23] S. Ahn, S. Lee, and W. S. Warren, Mol. Phys. **95**, 769 (1998).
[24] J. Zhong, Z. Chen, and E. Kwok, Magn. Reson. Med. **43**, 335 (2000).
[25] R. T. Branca, G. Galiana, and W. S. Warren, J. Chem. Phys. **129**, 054502 (2008).
[26] J. Kurhanewicz, D. B. Vigneron, K. Brindle, E. Y. Chekmenev, A. Comment, C. H. Cunningham, R. J. Deberardinis, G. G. Green, M. O. Leach, S. S. Rajan, R. R. Rizi, B. D. Ross, W. S. Warren, and C. R. Malloy, Neoplasia **13**, 81–97 (2011).
[27] W. S. Warren, S. Lee, W. Richter, and S. Vathyam, Chem. Phys. Lett. **247**, 207–214 (1995).
[28] C. Cai, Y. Lin, S. Cai, H. Sun, J. Zhong, and Z. Chen, J. Chem. Phys. **136**, 094503 (2012).
[29] R. Bowtell, private communication (2011).
[30] R. T. Branca and W. S. Warren, Magn. Reson. Med. **65**, 313 (2011).